Simultaneous detection of the acoustic-field aberration and Doppler shift in forward acoustic scattering*

Chuan-Lin He(何传林)[1,2], Kun-De Yang(杨坤德)[1,2,†], Yuan-Liang Ma(马远良)[1,2], and Bo Lei(雷波)[1,2]

[1] *Key Laboratory of Ocean Acoustics and Sensing (Northwestern Polytechnical University), Ministry of Industry and Information Technology, Xi'an* 710072, *China*

[2] *School of Marine Science and Technology, Northwestern Polytechnical University, Xi'an* 710072, *China*

(Received 9 May 2016; revised manuscript received 1 August 2016; published online 30 November 2016)

The aberration in the received acoustic field and the Doppler shift in the forward scattered field are simultaneously induced when a submerged target crosses the source–receiver line. Formulations for the two variations are developed upon an ideal forward scattering configuration. Both the field aberration and the Doppler shift are expressed as functions of the same argument — the target motion time. An experimental validation was carried out in a tank, in which the continuous wave was transmitted. The field aberration and the Doppler shift were extracted from the collected data by the simple Hilbert transform and a hybrid technique, respectively. The measured aberration and Doppler shift agree with the theoretical results. Simultaneous detection outputs are beneficial to enhance the reliability on target detection by providing both the aberrations in the received acoustic field and the Doppler shift in the forward scattered field.

Keywords: forward scattering detection, Doppler shift detection

PACS: 43.30.+m, 43.35.+d **DOI:** 10.1088/1674-1056/26/1/014301

1. Introduction

Forward acoustic scattering detection[1,2] is aimed at detecting a target crossing the source–receiver line. In this configuration, the scattered acoustic field interferes with the direct blast and is difficult to separate from the latter. However, the forward scattering target strength is generally higher than that in the backward direction,[3] particularly for aspect-dependent targets. The aberrations in the received acoustic field caused by the interference effect between the forward scattered field and the direct blast have been utilized to detect an intruder. Gillespie[4] exploited the matched filter technique to obtain the fluctuation of the received field in the forward acoustic scattering. Song[5] introduced the time reversal mirror (TRM) into an underwater acoustic barrier and achieved target detection by using the acoustic energy enhancement in the quiescent region of the TRM. Folegot[6] developed a ray-model-based algorithm to realize simultaneous detection and localization of multiple submerged targets crossing an acoustic barrier. Sabra[7] exploited the principal component analysis (PCA) to process the received field matrix and then utilized the second principal component to present the received field aberration. Lei[8] combined the PCA with the turning point filtering and applied the hybrid scheme to the data on a short vertical line array collected in a lake trial and then obtained the enhanced aberration extraction effect. Moreover, they also proposed a range estimation method[9] based on forward scattering using two separated hydrophones. He[10] proposed a direct blast suppression approach based on adaptive filtering and generated a curve varying with the observation time to indicate the received field aberration.

However, most of the above studies are focused directly or indirectly on the aberrations in the received acoustic-field. The motion characteristics of the target have not been fully utilized. Since the positions of the source and the receiver are fixed, the direct blast must be zero in Doppler shift. Meanwhile, the forward scattered field must be Doppler-shifted due to the relative motion of the target to the source–receiver line. In the case of passive detection, the target moving induced Doppler shift makes the instantaneous frequency of the received signal vary with the target motion time. The closest point of approaching (CPA) is always used to describe the time-varying characteristics of the instantaneous frequency at the receiver.[11,12] The instantaneous frequency rate reaches its minimum value at the CPA. Target range and velocity estimation methods are usually developed based on this property.

In this context, the crossing point of the moving target on the source–receiver line is similarly employed to describe the time-varying characteristics of the Doppler shift in the forward scattered field. A simultaneous detection scheme is proposed to represent the received acoustic-field aberration and forward scattered Doppler shift. Theoretical expressions are derived based on a simple forward scattering model, followed by an experimental validation conducted in an anechoic tank.

*Project supported by the National Natural Science Foundation of China (Grant Nos. 11174235 and 61571366).

†Corresponding author. E-mail: ykdzym@nwpu.edu.cn

© 2017 Chinese Physical Society and IOP Publishing Ltd

2. Theoretical analysis and simulation

2.1. Theoretical analysis

Figure 1 shows a submerged target crossing the bistatic source–receiver line, the length of which is represented by L. The length of the incident acoustic-path from the source to the target is denoted by $r_{\rm st}$, and that of the scattered acoustic-path from the target to the receiver is denoted by $r_{\rm tr}$. The target crosses the source–receiver line along a straight track at a constant velocity v. The intersection angle between the target track and the source–receiver line is denoted by α, meanwhile the crossing-point on the source–receiver line is labeled as C. The range from point C to the receiver is denoted by $L_{\rm tr}$. In the process of the target crossing, the bistatic angle β changes with the target position.

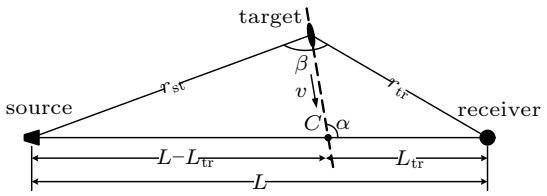


Fig. 1. Diagram of a submerged target crossing the source–receiver line (top-down view).

If the target crosses the source–receiver line at time $t_{\rm cb}$, then the distance from the target to the source–receiver line at an arbitrary moment t can be expressed by $v|t_{\rm cb}-t|$. Therefore, $r_{\rm st}$ and $r_{\rm tr}$ can be obtained in accordance with simple geometric relationships

$$\begin{aligned} r_{\rm st}(t) &= \sqrt{(L-L_{\rm tr})^2+v^2(t_{\rm cb}-t)^2+2(L-L_{\rm tr})v(t_{\rm cb}-t)\cos\alpha}, \\ r_{\rm tr}(t) &= \sqrt{L_{\rm tr}^2+v^2(t_{\rm cb}-t)^2-2L_{\rm tr}v(t_{\rm cb}-t)\cos\alpha}. \end{aligned} \tag{1}$$

The acoustic-path length for the forward scattered field is

$$r_{\rm f}(t) = r_{\rm st}(t)+r_{\rm tr}(t). \tag{2}$$

The corresponding acoustic-path length for the direct blast is L.

It is seen from Eqs. (1) and (2) that the acoustic-path of the forward scattered field is related to the target motion time. These formulas from which the received field aberration and the Doppler shift are derived constitute the basis of the theoretical analysis in this context.

According to Fig. 1, application of the law of cosine generates the bistatic angle β

$$\beta(t) = \cos^{-1}\left(\frac{r_{\rm st}^2(t)+r_{\rm tr}^2(t)-L^2}{2r_{\rm st}(t)\,r_{\rm tr}(t)}\right). \tag{3}$$

The arrival-time difference $\tau(t)$ of the forward scattered field referred to the direct blast is obtained from Eq. (1)

$$\tau(t) = \frac{r_{\rm f}(t)-L}{c}. \tag{4}$$

For the target with a given shape illuminated by an incident wave with a known frequency, the scattering pattern is dominated by the bistatic angle β. At the receiver, the interference effect between the forward scattered field and the direct blast is dominated by $\tau(t)$. Therefore, the received acoustic-field $p_{\rm r}(\beta(t),\tau(t))$ is the coherent sum of the forward scattered field $p_{\rm s}(\beta(t),\tau(t))$ and the direct blast $p_{\rm d}(\beta(t),\tau(t))$,

$$p_{\rm r}(\beta(t),\tau(t)) = p_{\rm s}(\beta(t),\tau(t))+p_{\rm d}(\beta(t),\tau(t)). \tag{5}$$

The Doppler shift of the forward scattered field is defined as[13]

$$f_{\rm d} = -\frac{1}{\lambda}\left[\frac{{\rm d}r_{\rm st}}{{\rm d}t}+\frac{{\rm d}r_{\rm tr}}{{\rm d}t}\right], \tag{6}$$

where λ is the wavelength of the incident wave. Substitution of Eq. (1) into Eq. (6) gives

$$f_{\rm d} = \frac{1}{\lambda}\left[\frac{v^2(t_{\rm cb}-t)+(L-L_{\rm tr})v\cos\alpha}{\sqrt{(L-L_{\rm tr})^2+v^2(t_{\rm cb}-t)^2+2(L-L_{\rm tr})v(t_{\rm cb}-t)\cos\alpha}}+\frac{v^2(t_{\rm cb}-t)-L_{\rm tr}v\cos\alpha}{\sqrt{L_{\rm tr}^2+v^2(t_{\rm cb}-t)^2-2L_{\rm tr}v(t_{\rm cb}-t)\cos\alpha}}\right]. \tag{7}$$

Equation (7) indicates that when the target is just located at the crossing point ($t=t_{\rm cb}$), the corresponding Doppler shift is exactly zero. Moreover, the cross-term for $\alpha\neq\pi/2$ (an oblique crossing) makes the Doppler shift curve more complex than that case for $\alpha=\pi/2$ (a vertical crossing). It is seen from Eqs. (5) and (7) that aberration in the received field and Doppler shift in the forward scattered field exist simultaneously when a submerged target is crossing the source–receiver line, and both the received acoustic field and the forward scattered Doppler shift can be expressed as functions of the target motion time.

2.2. Simulations for simultaneous detection

As shown in Fig. 2, an aluminum spherical shell is illuminated by a spherical wave emitted from a point source located at S which is $r_{\rm st}$ apart from the shell center. The origin of the coordinate system is located at the shell center. The spherical shell is filled with air. The inner and outer radii of the spherical shell are denoted by a and b, respectively. The angle θ is called the scattering angle, where $\theta=0$ corresponds to the forward scattering and $\theta=\pi$ corresponds to the backward scattering. The scattering angle and the bistatic angle satisfy $\theta+\beta=\pi$. The field point located at P records the received

acoustic field.

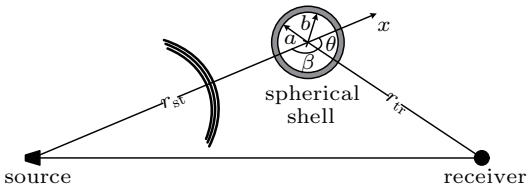


Fig. 2. Diagram of forward acoustic scattering from an aluminum spherical shell illuminated by a spherical wave.

According to Eqs. (1) and (3), the incident and the scattered acoustic fields can be expressed as series of spherical functions[14]

$$p_{\mathrm{inc}}\left(r_{\mathrm{st}}(t), r_{\mathrm{tr}}(t), \beta(t)\right) = \frac{\mathrm{e}^{\mathrm{i}kr_{\mathrm{st}}(t)}}{r_{\mathrm{st}}(t)} \sum_{n=0}^{+\infty} (2n+1)\,\mathrm{i}^n j_n\left(kr_{\mathrm{tr}}(t)\right) P_n\left[\cos\left(\pi-\beta(t)\right)\right], \quad (8)$$

$$p_{\mathrm{sct}}\left(r_{\mathrm{tr}}(t), \beta\right) = \sum_{n=0}^{+\infty} (2n+1)\,\mathrm{i}^n A_n h_n^{(1)}\left(kr_{\mathrm{tr}}(t)\right) P_n\left[\cos\left(\pi-\beta(t)\right)\right], \quad (9)$$

where $\mathrm{i}=\sqrt{-1}$, k is the wavenumber in the outer medium; j_n is the spherical Bessel function, $h_n^{(1)}$ is the spherical Hankel function of the first kind; and A_n is the coefficient to be determined from the conditions on the target (outer and inner) boundary. Substitution of Eqs. (8) and (9) generates the received acoustic field at point P

$$p_{\mathrm{r}}(t) = \sum_{n=0}^{+\infty} (2n+1)\,\mathrm{i}^n \left[\frac{\mathrm{e}^{\mathrm{i}kr_{\mathrm{st}}(t)}}{r_{\mathrm{st}}(t)} j_n\left(kr_{\mathrm{tr}}(t)\right) + A_n h_n^{(1)}\left(kr_{\mathrm{tr}}(t)\right)\right] \times P_n\left[\cos\left(\pi-\beta(t)\right)\right]. \quad (10)$$

Since the bistatic angle and the acoustic path are both related to the target position, the received field $p_{\mathrm{r}}(t)$ is also a function of the target motion time.

Let $f_{\mathrm{c}}=50$ kHz, $L=14$ m, $L_{\mathrm{tr}}=9$ m, $t_{\mathrm{cb}}=20$ s, and the aluminum spherical shell crosses the source–receiver line at a constant velocity $v=0.35$ m/s. The intersection angle α is chosen to be $\pi/6$, $\pi/3$, $\pi/2$, and $5\pi/6$ respectively. The aberration in the received field and the Doppler shift for the forward scattered field are calculated from Eqs. (10) and (7), and are shown together in Fig. 3. The longitudinal coordinate t_{mov} represents the target motion time. The latitudinal coordinates p_{r} in the upper panel and f_{d} in the lower panel represent the normalized received acoustic-field level (in dB) and the forward scattered Doppler shift (in Hz).

The maximum aberration is observed occurring at the time the target is crossing the source–receiver line due to the fact that the forward scattered energy has the peak value at this moment. The farther the target departs from the source–receiver line, the weaker the aberrations are. Meanwhile, the Doppler shift changes from positive to negative when the target crosses the source–receiver line and is exact zero when the target locates exactly at the cross-point. Moreover, the patterns of the field aberration and the Doppler shift are related to the target track. For the vertical crossing case, both the acoustic-field aberration and the Doppler shift reveal their symmetries of the crossing time t_{cb} as shown in Fig. 3(c), whereas the patterns become complicated as the track deviates from the vertical case.

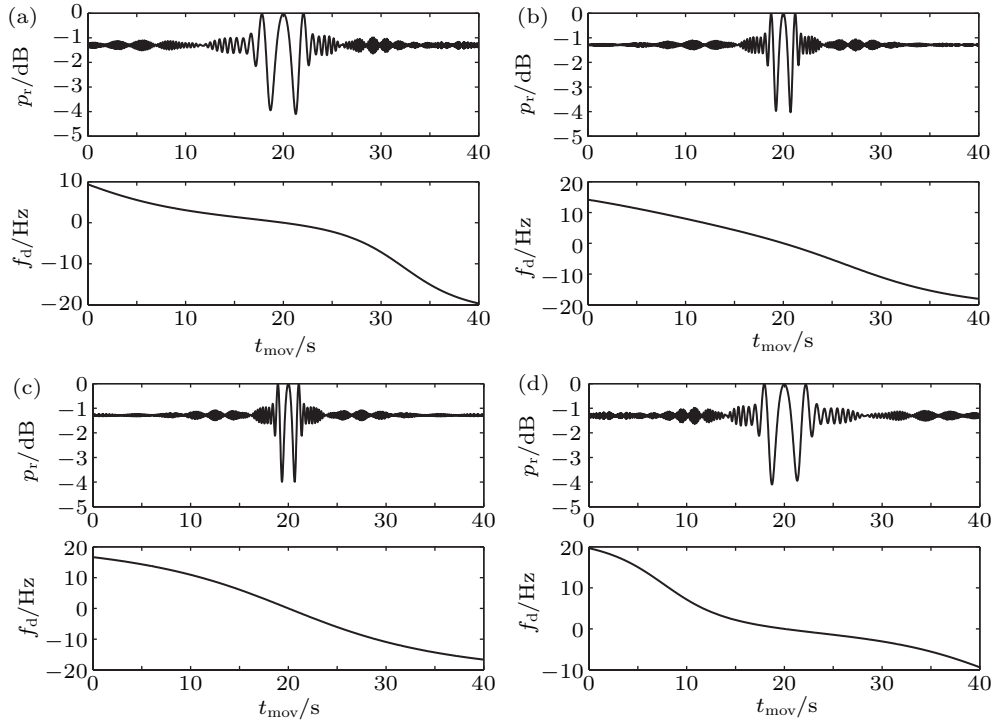


Fig. 3. Simultaneous detection output of the received acoustic-field aberration and the forward scattered Doppler shift for an aluminum spherical shell with (a) $\alpha=\pi/6$, (b) $\alpha=\pi/3$, (c) $\alpha=\pi/2$, and (d) $\alpha=5\pi/6$.

3. Experimental validation

3.1. Configuration

An experiment was conducted in the anechoic tank (20 m×8 m×7 m), as shown in Fig. 4(a). The transmitter, the target, and the hydrophone were deployed at the same depth of 3 m. The hydrophone was about 14.2 m apart from the transmitter. An aluminum spherical shell (shown in Fig. 4(b)) was used as the target, of which the inner radius $a = 0.09$ m and the outer one $b = 0.1$ m. In the experiment, the target crossed the source–receiver line along two tracks (labeled as A and B). The two tracks shared the same length but the opposite orientations. The target motion time for each track was about 20 s.

The target velocity v was fixed to 0.35 m/s, which was kept constant due to the fixed power system. The source center frequencies were chosen to be 30 kHz and 50 kHz. The Doppler shifts generated in the tank experiment represent the cases in which the target crosses the source–receiver line at a velocity of 5 knots illuminated by signals centered at 2.1 kHz and 3.0 kHz, respectively. The duration of the transmitting was about 65 s, which was three times longer than the duration of target motion.

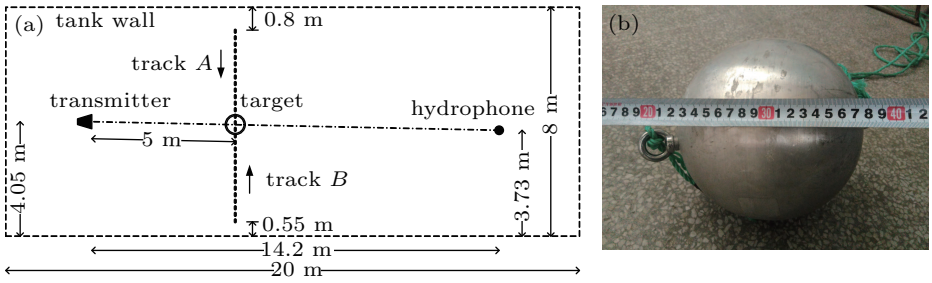


Fig. 4. (color online) Diagrams of the experiment: (a) top-down view layout, (b) target physical map.

3.2. Extraction of the acoustic-field aberration

Since the continuous wave is transmitted, the field aberration in the receiver can be directly represented by the envelope of the received field. The Hilbert transform is employed herein to extract the envelope in the received acoustic field. Figures 5(a) and 5(b) present the measured envelopes in tracks A and B for the source frequency 30 kHz, while figures 5(c) and 5(d) show the corresponding envelopes for 50 kHz. Meanwhile, the theoretical envelopes are also given in Fig. 5 by solid blue lines. These theoretical curves are calculated based on the vertical crossing for simplicity. The parameters used in the calculation are consistent with those in the experiment.

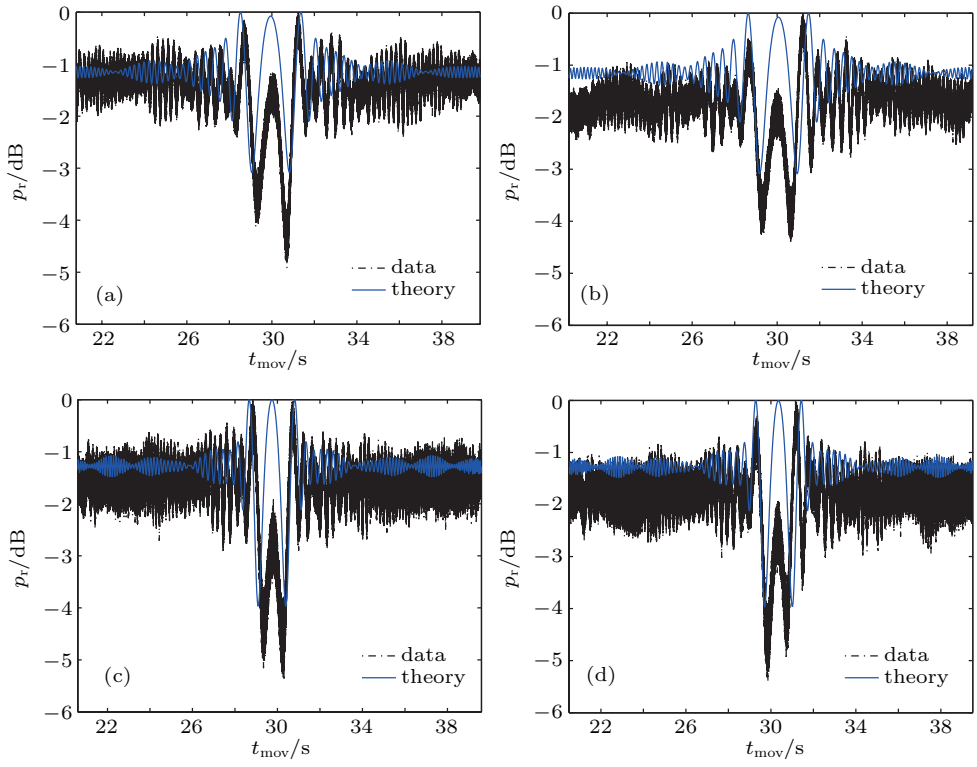


Fig. 5. (color online) Normalized acoustic-field aberrations in (a) track A, (b) track B for the source frequency 30 kHz; and in (c) track A, (d) track B for 50 kHz.

In Fig. 5(a), the measured envelope exhibits an approximated symmetry due to the fact that the target trajectory is approximately symmetric about the crossing-point. The closer the target is to the source–receiver line, the larger the fluctuation is. The magnitude of the aberration is around 4 dB. A similar phenomenon is observed from Fig. 5(b), except that the environment-induced fluctuations are relatively large. After the source frequency increases to 50 kHz, two variations are observed in the envelope. The first one is the enhanced aberration magnitude; the other is the shortened aberration duration. The reason is that the forward scattered energy beam is narrowed in width while strengthened in magnitude. Therefore, the magnitude of the aberration for 50 kHz is about 5 dB, which is a little larger than that for 30 kHz. The measured envelopes agree with the theoretical curves at aspects of aberration duration, pattern, and aberration magnitude during the period of the target crossing the source–receiver line. The maximum discrepancy between the measured and the theoretical envelopes is observed at the moment corresponding to the crossing-point, at which the interference effect between the forward scattered field and the direct blast is sensitive to factors such as target's practical depth and time-delay difference. These factors are difficult to be measured exactly in the experiment. It should be noted that the sound absorption is ignored in the theoretical calculation.

3.3. Extraction of the Doppler shift

The received field consists of both the direct blast and the forward scattered field, in which the two components interfere totally with one another. The simulated Doppler shift in Fig. 3 is relatively small, of which the magnitude decreases as the target approaches the source–receiver line. In the spectrum of the received acoustic-field, the direct blast corresponds to the main-lobe, whereas the forward scattered spectrum must be contained in the side-lobes due to the Doppler-shift. Therefore two problems should be overcome to extract the forward scattered Doppler shift: one is that the strength of the forward scattered field is much smaller than that of the direct blast; the other is that the Doppler shift contained in the forward scattered field is small and is sensitive to the target position. A hybrid scheme combining the sliding Blackman window function with fast Fourier transform (FFT) is proposed to extract the Doppler shift. The time domain expression and the corresponding spectrum for the Blackman window are given by[15]

$$\begin{aligned} w(n) &= 0.42 - 0.5\cos\left(\frac{2\pi n}{N}\right) + 0.08\cos\left(\frac{4\pi n}{N}\right), \\ &\quad (n = 0, 1, \ldots, N-1), \qquad (11) \\ W\left(\mathrm{e}^{\mathrm{i}\omega}\right) &= 0.42U(\omega) + 0.25\left[U\left(\omega - \frac{2\pi}{N}\right)\right. \\ &\quad \left. + U\left(\omega + \frac{2\pi}{N}\right)\right] \\ &\quad + 0.04\left[U\left(\omega - \frac{4\pi}{N}\right) + U\left(\omega + \frac{4\pi}{N}\right)\right], \qquad (12) \end{aligned}$$

where

$$U(\omega) = \mathrm{e}^{\mathrm{i}\omega/2}\frac{\sin(\omega N/2)}{\sin(\omega/2)}. \qquad (13)$$

The shape and the amplitude spectrum of a Blackman window function consisting of 100 samples are presented in Figs. 6(a) and 6(b), respectively. Compared with the commonly used rectangular window function, the side-lobe level of the Blackman window is significantly lowered to −58 dB. In data processing, the window length is chosen to be 10 s, providing a frequency (or Doppler) resolution of 0.1 Hz. The side-lobe low level is guaranteed by the characteristics of the Blackman window.

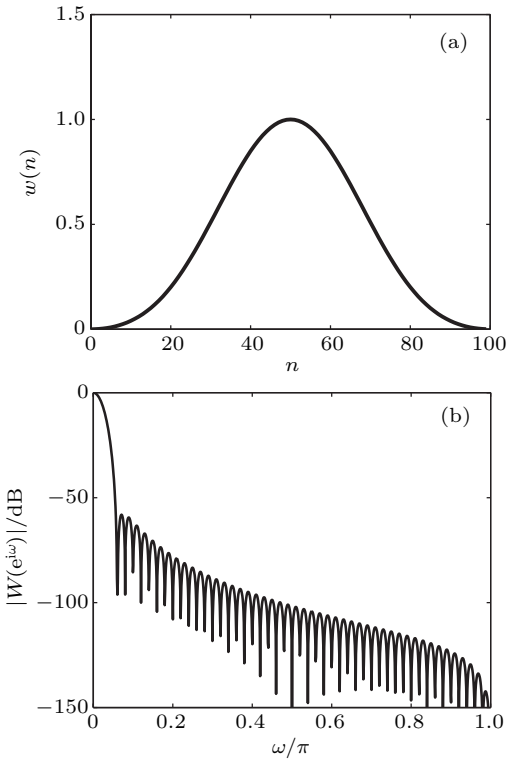


Fig. 6. Description of the Blackman window function: (a) the shape, (b) the amplitude spectrum.

There are about 273 data segments truncated by the Blackman window sliding along the total data stream with a step length of 0.2 s. The normalized amplitude spectrum (in dB) for every data segment is then stacked in accordance with the observation time, forming the final Doppler–time image. Figures 7(a) and 7(d) depict the Doppler–time images corresponding to Figs. 5(a)–5(d), respectively. The longitudinal coordinate t_{obv} corresponds to the observation time, which includes the target motion time.

The zero-Doppler straight striation is related to the direct blast, since the relative positions of the source and the receiver are fixed. The Doppler striation varying with observation time is exactly caused by the forward scattered field. The measured Doppler striation agrees with the theoretical curve

in magnitude, duration time, and tendency. Unlike the theoretical curve, the energy distribution along the Doppler striation is not uniform. When the target is far from the source–receiver line, the Doppler shift is large in magnitude whereas the corresponding scattered field is weak in intensity. When the target is near or located at the source–receiver line, the Doppler shift is around zero, but the scattered field is rather intensive. This phenomenon can be easily explained by the directionality of the forward scattered energy. This kind of Doppler-extraction approach is only suitable for the continuous wave.

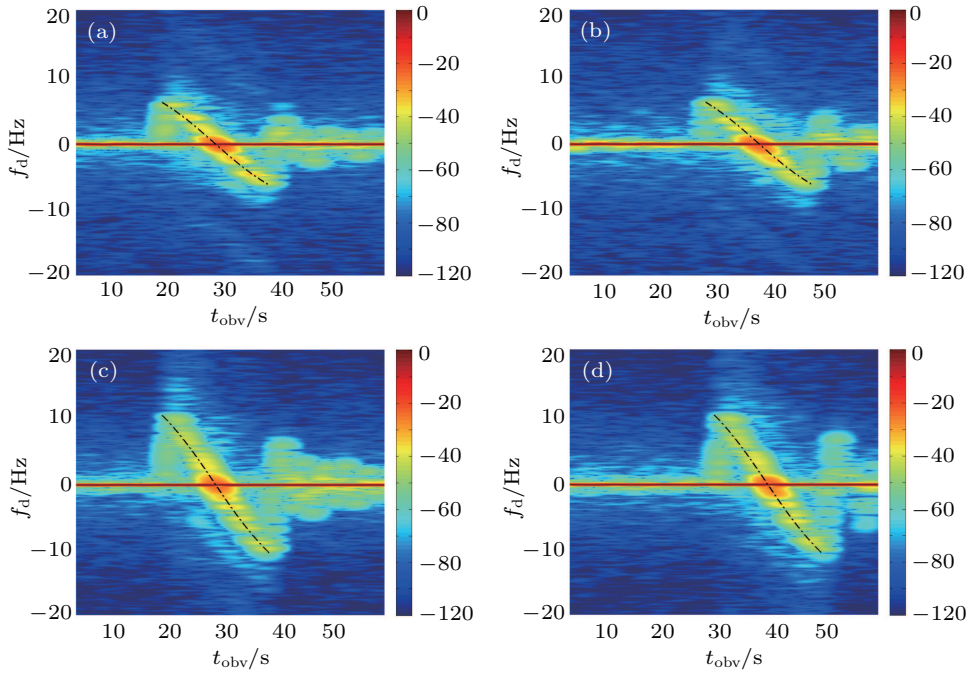


Fig. 7. (color online) Comparisons of the measured Doppler shift (color contour) with the theoretical one (the dashed-dotted line) in (a) track *A*, (b) track *B* for 30 kHz; and in (c) track *A*, (d) track *B* for 50 kHz.

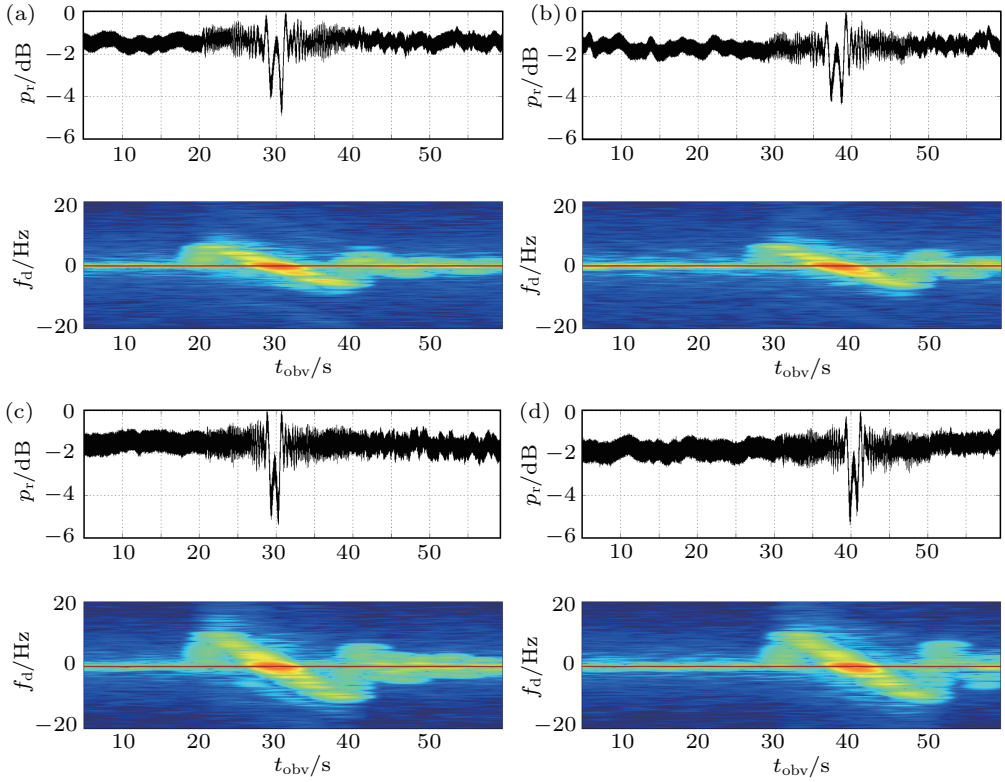


Fig. 8. (color online) Simultaneous detection results of the received acoustic-field aberration and the forward scattered Doppler shift in (a) track *A*, (b) track *B* for 30 kHz; and in (c) track *A*, (d) track *B* for 50 kHz.

3.4. Simultaneous detection results

It is seen from the above theoretical analysis, simulations, and experimental verifications that when a submerged target crosses the source–receiver line, the received acoustic-field aberration and the forward scattered Doppler shift are simultaneously induced and can be represented by functions that share the same argument — the target motion time. Simultaneous application of the approaches proposed in Subsections 3.2 and 3.3 to the same received acoustic field generates the joint representation of the acoustic-field aberration and the Doppler shift, where they span the same observation time. Figure 8 shows the simultaneous detection results, corresponding to those in Figs. 5 and 7. When there is no target (in this case the target is static), only fluctuations caused by the environment are observed in the envelope. Correspondingly, there is only the zero-Doppler straight striation in the Doppler–time image. As the target approaches and crosses the source–receiver line, the aberrations on the envelope are strengthened. At the same time, a Doppler striation arises and decreases with the target motion time. After the target departs from the source–receiver line, the aberrations are weakened and then disappear. The received envelope recovers to the state before the target crossing. In the Doppler image, the Doppler striation crosses the zero-Doppler straight line and converts from positive to negative. Finally, the Doppler striation vanishes after the target stops moving, and only the zero-Doppler straight line exists.

In the published literature upon forward scattering detection, results only provide direct or indirect information on the received acoustic-field aberration. The simultaneous detection is beneficial to enhance the reliability on target detection, for providing not only the aberrations in the received field but also the Doppler shift of the forward scattered field.

4. Consideration of the real scenario

In the tank experiment, the environment is rather ideal for its lower fluctuation. Meanwhile, the signal-to-noise ratio at the receiver is high due to the limited source–receiver distance. According to the sonar equation, the direct blast level at the receiver can be expressed by

$$DBL = SL - TL_{\mathrm{sr}}, \tag{14}$$

where SL is the source level (in dB) and TL_{sr} is the transmission loss from the source to the receiver. Similarly, the forward scattered wave level is

$$FSL = SL - TL_{\mathrm{st}} + TS_{\mathrm{f}} - TL_{\mathrm{tr}}, \tag{15}$$

where TL_{st} and TL_{tr} are the transmission losses from the source to the target and from the target to the receiver, respectively. TS_{f} is the target strength in the forward scattering direction and is usually evaluated by

$$TS_{\mathrm{f}} = 20\log_{10}\left(\frac{A}{\lambda}\right), \tag{16}$$

where A is the projected cross-section area. The variable signal-to-direct-blast ratio is defined herein to denote the signal power ratio of the forward scattered wave to the direct blast, and is expressed as

$$\begin{aligned} SDR &= FSL - DBL \\ &= 20\log_{10}\left(\frac{A}{\lambda}\right) + TL_{\mathrm{sr}} - TL_{\mathrm{st}} - TL_{\mathrm{tr}}. \end{aligned} \tag{17}$$

For an ideal case where the transmission loss is dominated by the cylindrical spreading loss, let $L_{\mathrm{tr}}/L = \gamma$, $\gamma \in (0,1)$, then equation (17) becomes

$$SDR = 20\log_{10}\left(\frac{A}{\lambda}\right) + 10\log_{10}\left[\frac{1}{\gamma(1-\gamma)}\right] - 10\log_{10}L. \tag{18}$$

Equation (18) indicates that SDR is dependent on the target position in the source–receiver line. In the tank experiment, SDRs for 30 kHz and 50 kHz are estimated to be -9.1 dB and -4.7 dB, respectively.

After the processing of direct blast suppression, the signal power ratio of the forward scattered wave to the direct blast is given by

$$SDR_{\mathrm{o}} = SDR + PG, \tag{19}$$

where PG is the processing gain from direct blast suppression. In present, almost all the studies concerned with forward acoustic scattering are focused on the variable PG. However, in reality the distance between the source and the receiver may be several kilometers or even tens of kilometers. Therefore, the signal-to-noise ratio for the direct blast may be very low and the aberrations induced by the forward scattered wave are probably overwhelmed by the environment-induced fluctuations.

5. Discussion and conclusion

The aberration in the received acoustic-field and the Doppler shift in the forward scattered field are simultaneously induced when a submerged target is crossing the source–receiver line. Formulations for the two variations are developed upon an ideal forward scattering configuration. Both of the field aberration and the Doppler shift are expressed as functions of the same argument – the target motion time. An experimental validation was carried out in a tank, in which the continuous wave was adopted as the source signal. The field aberration was presented by the envelope fluctuation extracted by the simple Hilbert transform, whereas the Doppler shift was extracted by a hybrid technique combining the sliding Blackman window function and fast Fourier transform. The measured aberration and Doppler shift agree with the theoretical

results. Simultaneous detection outputs are beneficial to enhance the reliability of target detection by providing both the aberrations in the received acoustic field and the Doppler shift in the forward scattered field.

Though the formulation and experiment are rather simple, the basic physics principles indicated by the results make common senses. Further research should be conducted in two aspects: modeling in ocean waveguide and designing the waveforms suitable for the simultaneous detection.

References

[1] Lei B, Yang K D and Ma Y L 2010 *Chin. Phys. B* **19** 054301
[2] Lei B, Ma Y L and Yang K D 2011 *Chin. Phys. Lett.* **28** 034302
[3] Urick R J 1983 *Principles of Underwater Sound* (2nd Edn.) (New York: McGraw-Hill) pp. 306–327
[4] Gillespie B, Rolt R, Edelson G, Shaffer R and Hursky P 1997 *Acoust. Imag.* **23** 501
[5] Song H, Kuperman W A, Hodgkiss W S, Akal T and Guerrini P 2003 *IEEE J. Ocean. Eng.* **28** 246
[6] Folegot T, Martinelli G, Guerrini P and Stevenson J M 2008 *J. Acoust. Soc. Am.* **124** 2852
[7] Sabra K G, Conti S, Roux P, Akal T, Kuperman W A, Stevenson J M, Tesei A and Guerrini P 2010 *J. Acoust. Soc. Am.* **127** 3430
[8] Lei B, Yang K D and Ma Y L 2014 *J. Acoust. Soc. Am.* **136** 2998
[9] Lei B, Yang K D and Ma Y L 2012 *J. Acoust. Soc. Am.* **132** EL284
[10] He C L, Yang K D, Ma Y L and Lei B 2015 *J. Acoust. Soc. Am.* **138** EL293
[11] Ferguson B G and Quinn B G 1994 *J. Acoust. Soc. Am.* **96** 821
[12] Quinn B G 1995 *J. Acoust. Soc. Am.* **98** 2560
[13] Cherniakov M 2007 *Bistatic Radar: Principles and Practice* (New York: John Wiley & Sons Ltd) p. 411
[14] Gaunaurd G C and Werby M F 1987 *J. Acoust. Soc. Am.* **82** 2021
[15] Oppenheim A V and Schafer R W 2009 *Discrete-time Signal Processing* (New Jersey: Prentice-Hall) pp. 533–538